

ProDehaze: Prompting Diffusion Models Toward Faithful Image Dehazing

1st Tianwen Zhou*
Department of Computer Science
University College London
London, United Kingdom
tianwenzhou0521@ieee.org

2nd Jing Wang
R&D Center Beijing Lab
Sony China Ltd.
Beijing, China
JingD.Wang@sony.com

3rd Songtao Wu
R&D Center Beijing Lab
Sony China Ltd.
Beijing, China
Songtao.Wu@sony.com

4th Kuanhong Xu
R&D Center Beijing Lab
Sony China Ltd.
Beijing, China
Kuanhong.Xu@sony.com

Abstract—Recent approaches using large-scale pretrained diffusion models for image dehazing improve perceptual quality but often suffer from hallucination issues, producing unfaithful dehazed image to the original one. To mitigate this, we propose ProDehaze, a framework that employs internal image priors to direct external priors encoded in pretrained models. We introduce two types of *selective* internal priors that prompt the model to concentrate on critical image areas: a Structure-Prompted Restorer in the latent space that emphasizes structure-rich regions, and a Haze-Aware Self-Correcting Refiner in the decoding process to align distributions between clearer input regions and the output. Extensive experiments on real-world datasets demonstrate that ProDehaze achieves high-fidelity results in image dehazing, particularly in reducing color shifts. Our code is at <https://github.com/TianwenZhou/ProDehaze>.

Index Terms—Image Restoration, Diffusion Models, Image Dehazing, Visual Prompt Learning

I. INTRODUCTION

Restoring a clean image from a hazy input is a long-standing yet challenging ill-posed problem. Dehazing is crucial for various applications, including autonomous driving [1], where clear visibility is essential for safe navigation, and aerial photography [2] or remote sensing [3], which require haze removal for accurate environmental monitoring. Significant progress has been made through the advent of deep learning-based methods [4–8], which employs deep neural networks to either estimate parameters of the Atmospheric Scattering Model (ASM) [9, 10] or directly restore the dehazed image. These methods rely on synthetic hazy-clean image pairs for training, which often generalizes poorly to real scenes, as synthetic haze may not adequately represent the complexity and diversity of actual conditions. Recently, diffusion models [11, 12] have shown promising results in various image restoration tasks [13–15], including dehazing [16, 17].

Several studies [15, 18, 19] have successfully utilized *external* priors—specifically, generative priors embedded in large-scale pretrained diffusion models—to enhance the perceptual quality of restored images significantly. Unlike traditional learning-based methods, pretrained diffusion models exploit the inherent distribution of natural images, leading to superior generalization and improved photo-realism. Notably, powerful

text-to-image (T2I) models, such as Latent Diffusion Models (LDMs) [12], are often used to provide these external priors. The dehazing process is learned in the latent space through finetuning a pretrained denoising UNet. However, despite achieving high-quality results, these methods remain susceptible to *hallucination* issues [20]. Restored image may lack faithfulness, with inconsistencies in content or details compared to the original images, especially for severely degraded inputs. To address this, some methods [21] finetune the decoding process of the autoencoder in LDMs, yet they still struggle with color shifts and detail inconsistencies.

To mitigate hallucination issues in real-scene dehazing, this paper explores the use of *internal* image priors—statistics derived from within an input image—to direct the *external* priors of LDMs for faithful dehazing. We propose that these internal priors should be *selective* enough to identify critical areas in the input image essential for faithful dehazing. By prompting these priors into the pretrained LDMs, we aim to shift the models’ knowledge toward these areas, thereby enabling reliable restoration of hazy images.

Specifically, in the semantically-rich **latent space** of LDMs [12], we propose spatial structure signals as internal priors to guide the model’s emphasis on structure-rich areas. It is unveiled that these areas are more decomposable in the frequency domain than in the spatial domain [22]. Therefore, we derive prompts through frequency decomposition to indicate spatial cues for key areas. The prompts are then injected into the proposed Structure-Prompted Restorer (SPR) to enable the model to capture spatial correlations and enhance fidelity of the corresponding details. In the **decoding process**, we introduce a novel Haze-Aware Self-Correcting Refiner to ensure faithful decoding. We propose using a haze-aware prior to enhance the representation of clearer areas while minimizing the impacts of haze-dominant areas. A self-correction mechanism is then employed to promote alignment between the clearer regions of the input hazy image and the output dehazed image. This is achieved by inserting self-attention blocks into the decoder and re-weighting the attention maps using the haze-aware priors. Extensive experiments demonstrate the effectiveness of this self-correcting mechanism in reducing color shifts.

The contributions of this paper can be summarized as:

- We introduce using internal image priors to guide the

* This work was conducted during an internship at Sony China Ltd.

external knowledge of pretrained LDMs toward critical areas in hazy images, aiming to mitigate hallucination issues and thereby, produce faithful dehazed images.

- In the latent space, we prompt structural priors into the pretrained diffusion model to improve its capture of spatial correlations towards structural-rich areas, thereby reliably restoring the details of these areas.
- In the decoding process, we employ haze-aware priors and a self-correction mechanism to align distributions between clearer input regions and output image, effectively reducing color shifts.

II. RELATED WORKS

A. Image Dehazing

While prior-based dehazing methods utilize hand-crafted priors [23], deep learning approaches restore haze-free images in a data-driven manner. Early works employed neural networks to estimate intermediate parameters [24, 25] of ASM or directly predict dehazed images [4, 5]. However, these methods often degrade in performance with real-world hazy images. Recently, deep generative models, including CycleGAN-based domain adaptation strategies [26], have been explored for real-scene dehazing. Wu *et al.* [27] further utilize high-quality codebook priors from large-scale datasets to handle real-scene complexities. Nonetheless, these methods still face challenges with domain gap, hindering their real-world applicability.

B. Diffusion Models for Image Restoration

Diffusion models [11] have emerged with impressive results in image restoration tasks [13, 18, 19, 28], including dehazing [16, 17]. Early works [16] trained these models from scratch, limiting their ability to leverage the power of pretrained generative priors. Recent research has utilized pretrained LDMs [12] for restoration. For instance, Lin *et al.* [19] introduced DiffBIR, which integrates degradation removal and information regeneration modules within pretrained LDMs. Wang *et al.* [18] advanced this with a Controllable Feature Wrapping (CFW) module to balance fidelity and perceptual quality. Yang *et al.* [29] explored LDMs for dehazing, by investigating the semantic properties of hazy images in the latent space. However, these methods rely on generative priors obtained from external databases without effectively incorporating visual cues from input images, which can lead to hallucination artifacts and reduced fidelity in real-world scenarios.

C. Visual Prompt Learning

Prompt learning, originally developed in natural language processing (NLP) [30], has recently been adapted to low-level vision tasks to leverage task-specific priors [31–36]. Methods like SelfPromer [35] and PromptRestorer [36] utilize image priors, such as depth consistency or degradation-specific features, to guide restoration. However, these priors often lack selectivity in identifying critical areas in the input image for pretrained models to focus on, potentially diluting their effectiveness. Our work addresses this issue by prompting LDMs with highly selective image priors, enabling more faithful dehazing.

III. THE PROPOSED METHOD

A. Overview

Our proposed prompts selectively direct the external knowledge of pre-trained LDMs to image regions critical for faithful dehazing. We designed two types of prompts: in the latent space, the regions with fine structures are prioritized through a Structure-prompted Restorer to ensure faithfulness (Sec III-B); during subsequent decoding, heavily degraded areas are deprioritized using a Haze-aware Self-correcting Refiner (Sec III-C). An overview of the framework is presented in Fig. 1.

B. Structure-prompted Restorer (SPR)

In the latent space where pre-trained diffusion models encode rich semantics [12], we identify *selective* internal priors—fine structures, contours, and edges—that provide essential visual cues for semantic meaning. These elements, as shown in Supplementary Materials II, are more distinct in frequency domain than in image space. Moreover, high-frequency structures are more resilient to haze, as haze primarily carries low-frequency information [16]. Therefore, we propose using High-frequency prompts to guide the dehazing process.

Specifically, we utilize the Haar Feature Extractor (HFE), which is the Haar Discrete Wavelet Transform (Haar DWT) [37] followed by a learnable convolution kernel. The Haar DWT extracts three high-frequency components ($\mathcal{G}_{LH} * x_{in}$, $\mathcal{G}_{HH} * x_{in}$, and $\mathcal{G}_{HL} * x_{in}$) from the input x_{in} . These components are then fused and processed with a point-wise convolution kernel to produce the high-frequency feature:

$$x_{high} = \text{conv}_{1 \times 1}[(\mathcal{G}_{LH} * x_{in}) \oplus (\mathcal{G}_{HH} * x_{in}) \oplus (\mathcal{G}_{HL} * x_{in})] \quad (1)$$

Here, $*$ denotes a convolution operation, \oplus indicates channel-wise concatenation, and $\text{conv}_{1 \times 1}$ represents the point-wise convolution kernel. To enable the pretrained denoising UNet to capture high-frequency structural signals, we concatenate x_{high} and x_{in} in the latent space of LDM:

$$c_f = \mathcal{E}(x_{in}) \oplus \mathcal{E}(x_{high}) \quad (2)$$

where c_f represents the condition for diffusion model, \mathcal{E} denotes the VAE encoder. To leverage the external priors of denoising UNet, we adopt a method similar to [12, 38] by introducing an adaptor \mathcal{N} that creates a trainable copy of the UNet. This adaptor \mathcal{N} enables the injection of the conditioning prompt c_f into the diffusion process as structural guidance.

Finally, we finetune the diffusion model via optimizing following objective function:

$$\mathcal{L}_{SPR} = \mathbb{E}_{x_{in}, t, c_f, \epsilon \sim N(0,1)} [\|\epsilon - \epsilon_{\theta}(z_t, t, \mathcal{N}(c_f))\|_2^2] \quad (3)$$

where ϵ_{θ} denotes the pretrained denoising UNet. During finetuning, we only apply gradient descent to the learnable kernel $\text{conv}_{1 \times 1}$ and the adaptor \mathcal{N} while freezing the weights of ϵ_{θ} .

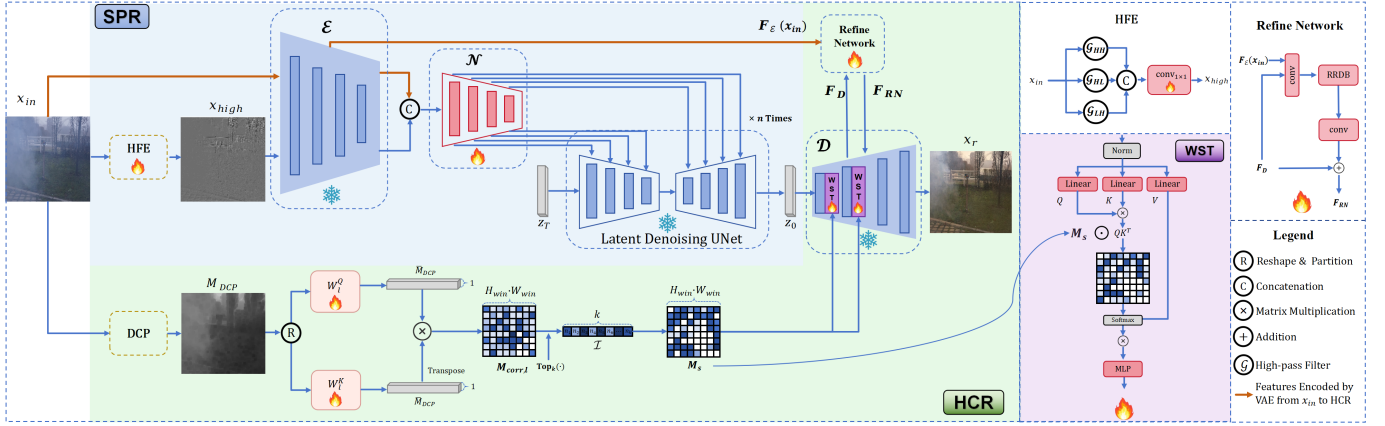


Fig. 1. **Framework of ProDehaze.** We employ a two-phase finetuning strategy for faithful dehazing. In the first phase, we train the Structure-Prompted Restorer (SPR) in the latent space using a structural prompt generated by a Haar Feature Extractor (HFE) from the hazy input x_{in} . It is then concatenated with the latent representation of x_{in} and injected into the trainable adapter \mathcal{N} to provide structural guidance. In the second phase, we finetune the Haze-aware Self-Correcting Refiner (HCR) in the decoding process. The haze-aware prompt, initialized by Dark Channel Prior (DCP), produces a sparse mask M_s that emphasizes the clearer areas in x_{in} . It is used to modulate the attention map of the window swin transformer (WST) in the decoder \mathcal{D} . Finally, \mathcal{D} and the refine network are jointly trained for better alignment between the clearer regions in x_{in} and the output x_r .

C. Haze-aware Self-correcting Refiner (HCR)

Despite the improved faithfulness of our SPR-boosted dehazing process in the latent space, the final dehazed image often diverges from the groundtruth, *i.e.*, *hallucination* dilemma. Previous works [21, 39] address the challenges by finetuning the decoder \mathcal{D} with a small refine network. Building on this approach, we propose a self-correction mechanism that leverages haze-aware priors within a hazy image to enhance fidelity. This is achieved by inserting several self-attention (SA) blocks into \mathcal{D} , modulated by priors that recognize haze density (see Fig.1). These priors are selective in prioritizing areas with thinner haze while deprioritizing areas with dense haze. Thus, self-correction is enabled by distribution alignment towards more reliable signals, such as clearer regions.

To initialize the haze-aware internal prior, we employ the Dark Channel Prior (DCP) [23], which provides an efficient yet approximate estimation of haze distribution within an image. From the input image x_{in} , we compute the DCP mask $M_{DCP} \in \mathbb{R}^{H \times W \times 1}$, where (H, W) represents the spatial dimensions of x_{in} . Higher values in M_{DCP} indicate regions with denser haze. The mask is then flattened into a 1D vector $\bar{M}_{DCP} \in \mathbb{R}^{N \times 1}$, where $N = H \times W$.

In the l -th block of the decoder \mathcal{D} , we compute a correlation map $M_{corr,l}$ to capture interactions among all elements in \bar{M}_{DCP} . This is achieved by applying the cross product between \bar{M}_{DCP} and its transposition, modulated through two learnable weight matrices $W_l^Q \in \mathbb{R}^{1 \times N_l}$ and $W_l^K \in \mathbb{R}^{1 \times N_l}$:

$$M_{corr,l} = (\bar{M}_{DCP} W_l^Q) \times (\bar{M}_{DCP} W_l^K)^T \quad (4)$$

where $N_l = H_l W_l$ denotes the size of the feature map in the l -th block. Then a top- k selection [40], denoted as $\text{Top}_k(\cdot)$, is applied to $M_{corr,l}$ to extract the indices of the k highest values in it:

$$\mathcal{I} = \{(i, j) \mid M_{corr,l}^{ij} \in \text{Top}_k(M_{corr,l})\} \quad (5)$$

We use the set of indices \mathcal{I} , corresponding to the k most haze-affected regions, to sparsify M_{corr} , yielding a sparsified mask M_s . The elements of M_s are computed as follows:

$$M_s^{ij} = \begin{cases} -\infty, & (i, j) \in \mathcal{I} \\ 1 - M_{corr}^{ij}, & (i, j) \notin \mathcal{I}. \end{cases} \quad (6)$$

This sparsification strategy selectively eliminates the negative impact of haze-dominant areas in M_{corr} by assigning $-\infty$, while emphasizing the representation of clearer areas by assigning a weight of $1 - M_{corr}^{ij}$. Next, M_s is injected to modulate the standard self-attention calculation in the Window Swin Transformer (WST) block in the decoder \mathcal{D} by:

$$\text{attn}(M_s) = \text{softmax}((QK^T) \odot M_s / \sqrt{N_l})V \quad (7)$$

where \odot denotes element-wise multiplication, and Q, K , and V are the Query, Key, and Value matrices of attention layer. Note that we adopt window Swin Transformer blocks [41] of size (H_{win}, W_{win}) for computation efficiency. Consequently, the dimensions of M_{DCP} are adapted to match this window size. The transformer blocks are inserted into the two lowest-resolution stages of \mathcal{D} . During training, we generate the latent vector z_0 from the finetuned SPR. Additionally, we extract multi-scale features $F_{\mathcal{E}}(x_{in})$ of the input x_{in} from the VAE encoder \mathcal{E} . The output dehazed image x_r is:

$$x_r = \mathcal{D}(z_0; R(F_{\mathcal{E}}(x_{in}), F_D), \text{attn}(M_s)) \quad (8)$$

where R represents the trainable refine network that aligns $F_{\mathcal{E}}(x_{in})$ and the decoder feature F_D , generating the refined feature F_{RN} . To train HCR, we minimize the following loss:

$$\mathcal{L}_{HCR} = \|x_r - x_{GT}\|_1 + \mathcal{L}_{VGG}(x_r, x_{GT}) + \mathcal{L}_{adv}(x_r, x_{GT}) \quad (9)$$

where x_{GT} denote the ground true image, \mathcal{L}_{VGG} and \mathcal{L}_{adv} are the VGG perceptual loss [42] and the adversarial loss [43].

TABLE I
QUANTITATIVE COMPARISON ON FIVE REAL-WORLD DATASETS, **BOLD** AND UNDERLINE INDICATE THE BEST AND THE SECOND-BEST, RESPECTIVELY

Dataset	Metrics	FCB	RIDCP	C2PNet	DEANet	FSNet	SFSNiD	DiffUIR	CASM	PromptIR	FPro	Ours
I-Haze	PSNR↑	17.35	<u>17.41</u>	16.70	16.54	17.13	16.18	16.75	17.12	16.07	16.69	21.69
	SSIM↑	<u>0.82</u>	0.79	0.77	0.78	0.78	0.74	0.78	0.80	0.76	0.77	0.87
	CIEDE↓	<u>11.53</u>	12.14	12.52	13.05	12.17	15.64	12.36	12.62	13.81	13.05	7.88
	CLIPQA↑	0.31	0.35	0.34	0.35	0.35	0.24	0.34	<u>0.36</u>	0.34	0.24	0.40
O-Haze	NIMA↑	5.01	<u>5.12</u>	4.45	4.55	4.38	4.00	4.43	5.10	4.72	4.77	5.27
	PSNR↑	17.39	16.74	16.53	16.53	16.01	<u>17.75</u>	15.33	17.64	16.41	17.08	18.73
	SSIM↑	0.80	0.76	0.70	0.69	0.67	0.66	0.65	0.77	0.68	0.71	0.77
	CIEDE↓	13.58	<u>12.03</u>	15.98	15.89	15.84	14.32	16.69	12.98	16.01	15.52	11.65
DenseHaze	CLIPQA↑	0.41	0.52	<u>0.44</u>	0.43	<u>0.44</u>	0.30	0.42	<u>0.44</u>	0.46	0.33	<u>0.44</u>
	NIMA↑	<u>5.12</u>	5.15	4.97	4.96	4.95	4.38	4.85	5.13	5.12	5.06	5.15
	PSNR↑	13.16	11.28	11.67	11.57	11.34	12.35	10.23	<u>13.98</u>	11.54	11.12	14.06
	SSIM↑	0.49	<u>0.49</u>	0.44	0.44	0.43	0.43	0.40	<u>0.50</u>	0.43	0.46	0.52
NhHaze	CIEDE↓	21.32	25.03	24.51	24.84	24.87	22.82	26.96	<u>18.58</u>	24.84	25.14	18.53
	CLIPQA↑	0.21	0.33	0.25	0.23	0.25	0.23	0.25	0.19	0.24	0.24	<u>0.31</u>
	NIMA↑	5.00	<u>5.24</u>	4.82	4.84	4.80	4.08	4.64	4.09	4.86	4.63	5.25
	PSNR↑	<u>14.17</u>	12.95	12.47	12.37	12.27	13.20	11.97	13.61	12.30	12.40	14.62
RTTS	SSIM↑	0.62	0.48	0.53	0.52	0.51	0.49	0.49	0.62	0.51	0.51	<u>0.58</u>
	CIEDE↓	<u>17.30</u>	19.91	21.86	18.59	21.48	20.17	21.63	17.98	21.77	21.66	16.73
	CLIPQA↑	0.39	0.49	0.42	0.40	<u>0.43</u>	0.35	0.40	0.42	0.49	0.37	<u>0.43</u>
	NIMA↑	5.56	5.76	5.65	5.60	<u>5.64</u>	4.94	5.56	5.08	<u>5.69</u>	5.62	5.61
RTTS	CLIPQA↑	0.23	0.34	0.32	0.31	<u>0.33</u>	0.28	<u>0.33</u>	0.30	<u>0.33</u>	0.32	0.34
	NIMA↑	4.52	<u>5.13</u>	5.03	5.02	4.97	4.67	5.02	5.02	4.96	5.01	5.14

IV. EXPERIMENTS

A. Experimental Settings

Datasets. For the training set, we utilize both the Indoor Training Set (ITS) and Outdoor Training Set (OTS) from the Realistic Single Image Dehazing (RESIDE) [44] benchmark. For the test sets, we select four commonly used datasets of paired hazy-clean images: I-Haze [45], O-Haze [46], DenseHaze [47], and NH-Haze [48]. Additionally, we include the RTTS [44] dataset, which contains only real-world hazy images without groundtruth, to evaluate the model’s dehazing performance for real scenes.

We utilize the ASM-based synthesis pipeline [16] to generate the synthetic pairs for training. To demonstrate the generalization capability of our model, we train exclusively on synthetic hazy-clean pairs from ITS and OTS, and evaluate directly on the test sets without any ad-hoc finetuning.

Evaluation. We adopt widely used reference-based metrics—PSNR, SSIM, and CIEDE [49]—to evaluate image distortion, structural similarity, and color difference, respectively, between the dehazed and groundtruth images. To further assess the perceptual quality of the dehazed images, we employ CLIPQA [21] and NIMA [50], which are non-reference image quality assessment metrics based on pretrained models.

Benchmark Comparison. We evaluate the performance of our proposed model against a range of state-of-the-art dehazing algorithms, focusing on diffusion-based methods (e.g. FCB [16], DiffUIR [28]), real-scene dehazing methods (e.g. RIDCP [27], CASM [8], SFSNiD [51]), image prompting (e.g. PromptIR [31], FPro [32]), as well as other state-of-the-art algorithms (e.g. C2PNet [52], DEANet [53], FSNet [54]). We specify our implementation strategy in Supplementary Materials I.

B. Quantitative Comparison

As presented in Table I, our proposed method consistently outperforms all baseline methods across the test datasets. Notably, referenced metrics such as PSNR, SSIM and CIEDE

TABLE II
ABLATION STUDY OF SPR AND HCR ON I-HAZE AND O-HAZE.

Exp.	Modules					I-Haze / O-Haze		
	Vanilla Adapter	Adaptor w/ SPR	Vanilla Refine Network	HCR w/o M_s	HCR w/ M_s	PSNR↑	SSIM↑	CIEDE↓
(a)	✓					17.36 / 16.43	0.74 / 0.46	13.29 / 16.22
(b)		✓				19.33 / 16.97	<u>0.86</u> / 0.48	10.02 / 14.96
(c)	✓		✓			19.90 / 18.35	<u>0.75</u> / <u>0.75</u>	<u>9.45</u> / 12.56
(d)		✓	✓			19.94 / 18.55	0.84 / <u>0.77</u>	10.47 / 12.54
(e)		✓		✓		<u>20.15</u> / <u>18.56</u>	0.84 / <u>0.77</u>	10.25 / <u>12.44</u>
(f)		✓			✓	21.69 / 18.73	0.87 / <u>0.77</u>	7.88 / 11.65

excel other methods significantly. This can be attributed to the effective integration of internal priors alongside external priors from the pre-trained LDM, which significantly enhances fidelity while preserving perceptual quality. As for real-world dehazing, our method demonstrates superiority on RTTS dataset, according to the improvements in the non-reference NIMA and CLIPQA metrics. Notably, even without finetuning on real-world hazy images, our approach achieves competitive results to RIDCP [27], which is tailored for such scenarios.

C. Qualitative Comparison

Fig. 2 presents a visual comparison of dehazing results against existing benchmark methods. On the I-Haze and O-Haze datasets, our method shows superior performance, delivering visually compelling results with significantly reduced haze residue. For the DenseHaze and NhHaze datasets, our approach effectively removes the majority of the haze and accurately restores the underlying structure of the input images. Notably, the proposed HCR module has substantially improved color fidelity, effectively correcting color bias and suppressing the hallucinated details from the pretrained LDMs. We provide visual results on RTTS in Supplementary Materials III.

D. Ablation Study

Effect of SPR. To show the importance of the proposed SPR, we present quantitative results in Table III and visual results in Fig.3. As shown in Table III (a) and (b), SPR significantly enhances performance across test sets compared to a vanilla

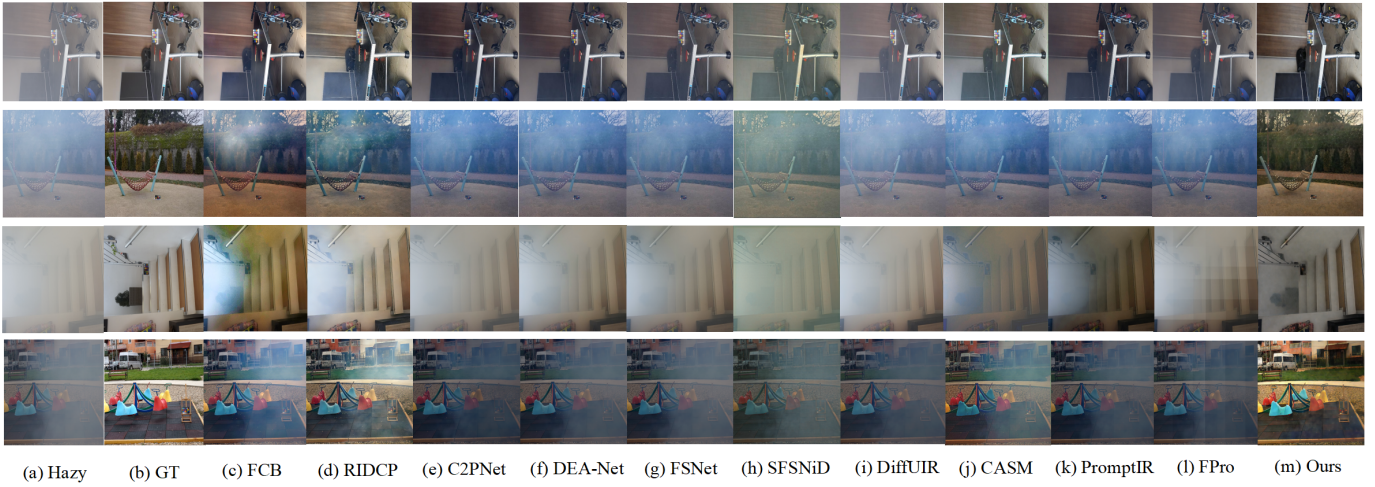


Fig. 2. Qualitative comparison of dehazing results with different methods. From top to bottom are the results on I-Haze, O-Haze, DenseHaze and NhHaze.

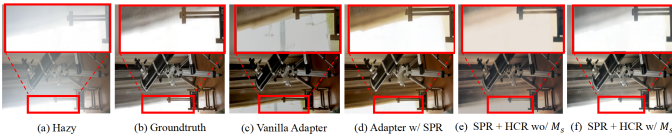


Fig. 3. Ablation study on the proposed method. (c) finetuning only the vanilla adapter \mathcal{N} . (d) finetuning SPR only. (e) finetuning both SPR and HCR, but without M_s modulation (f) full setting.

adapter without structural prompts. The visual results in Fig. 3(c) contain hallucinated details and incorrect content, while (d) exhibits a faithful restoration. Furthermore, as shown in Table III (c) and (d), such improvement persist after integrating a refine network. Overall, these findings validate the role of SPR in restoring faithful structural information via the proposed prompt. They demonstrate that high fidelity can be achieved in a well-prompted latent space, even without decoder refinement.

Effect of HCR. Table III (e) and (f) show that the HCR module markedly improves PSNR, underscoring its strength in enhancing faithfulness. The improvement in CIEDE further highlights HCR’s ability to mitigate color bias. Additionally, Table III (d) and (e) show that such improvement arises from M_s modulation via haze-aware prior, while merely inserting WST blocks yields only minimal impact on the results.

To further validate the effectiveness of haze-aware prior on color correction, we provide visual comparisons in Fig. 3. Without the haze-aware prior, noticeable color shifts are evident in Fig. 3(e). In contrast, the color bias is substantially reduced with the integration of haze-aware prior in Fig. 3(f).

V. CONCLUSION

We propose a novel real-world dehazing framework ProDehaze that directs external image priors within pretrained diffusion models with internal priors for faithful dehazing. Specifically, we design two selective priors to prompt the model: structural priors in the latent space and haze-aware prompts during decoding. These priors enable the pretrained model to

produce high-fidelity results with preserved structures, faithful details, and reduced color bias. Our framework demonstrates the effectiveness of guiding pretrained knowledge toward critical image areas for faithful restoration, offering a promising avenue for addressing other inverse problems.

REFERENCES

- [1] F. Tao, Q. Chen, Z. Fu, L. Zhu, and B. Ji, “Lid-net: A lightweight image dehazing network for automatic driving vision systems,” *Digital Signal Processing*, vol. 154, p. 104673, 2024.
- [2] A. Kulkarni and S. Murala, “Aerial image dehazing with attentive deformable transformers,” in *Proceedings of the IEEE/CVF Winter Conference on Applications of Computer Vision (WACV)*, Waikoloa, HI, USA, 2023, pp. 6294–6303.
- [3] J. Liu, S. Wang, X. Wang, M. Ju, and D. Zhang, “A review of remote sensing image dehazing,” *Sensors*, vol. 21, no. 11, p. 3926, 2021.
- [4] B. Li, X. Peng, Z. Wang, J. Xu, and D. Feng, “Aod-net: All-in-one dehazing network,” in *Proceedings of the IEEE International Conference on Computer Vision (ICCV)*, 2017, pp. 4770–4778.
- [5] Y. Song, Z. He, H. Qian, and X. Du, “Vision transformers for single image dehazing,” *IEEE Transactions on Image Processing*, vol. 32, pp. 1927–1941, 2023.
- [6] K. Chandrasegaran, N.-T. Tran, and N.-M. Cheung, “A closer look at fourier spectrum discrepancies for cnn-generated images detection,” in *Proceedings of the IEEE/CVF Conference on Computer Vision and Pattern Recognition (CVPR)*, 2021, pp. 7200–7209.
- [7] C. Li, C. Guo, J. Guo, P. Han, H. Fu, and R. Cong, “Pdr-net: Perception-inspired single image dehazing network with refinement,” *IEEE Transactions on Multimedia*, vol. 22, no. 3, pp. 704–716, 2019.
- [8] X. Wang, X. Chen, W. Ren, Z. Han, H. Fan, Y. Tang, and L. Liu, “Compensation atmospheric scattering model and two-branch network for single image dehazing,” *IEEE Transactions on Emerging Topics in Computational Intelligence*, vol. 8, no. 4, pp. 2880–2896, 2024.
- [9] H. Zhang and V. M. Patel, “Densely connected pyramid dehazing network,” in *Proceedings of the IEEE Conference on Computer Vision and Pattern Recognition (CVPR)*, 2018, pp. 3194–3203.
- [10] X. Zhao, K. Wang, Y. Li, and J. Li, “Deep fully convolutional regression networks for single image haze removal,” in *Proceedings of the 2017 IEEE Visual Communications and Image Processing (VCIP)*. IEEE, 2017, pp. 1–4.
- [11] J. Ho, A. Jain, and P. Abbeel, “Denoising diffusion probabilistic models,” *Advances in Neural Information Processing Systems (NeurIPS)*, vol. 33, pp. 6840–6851, 2020.
- [12] R. Rombach, A. Blattmann, D. Lorenz, P. Esser, and B. Ommer, “High-resolution image synthesis with latent diffusion models,” in *Proceedings of the IEEE/CVF Conference on Computer Vision and Pattern Recognition (CVPR)*, 2022, pp. 10 684–10 695.

- [13] B. Kawar, M. Elad, S. Ermon, and J. Song, “Denoising diffusion restoration models,” in *Advances in Neural Information Processing Systems (NeurIPS)*, vol. 35, 2022, pp. 23 593–23 606.
- [14] C. Saharia, J. Ho, W. Chan, T. Salimans, D. J. Fleet, and M. Norouzi, “Image super-resolution via iterative refinement,” *IEEE Transactions on Pattern Analysis and Machine Intelligence*, vol. 45, no. 4, 2023.
- [15] T. Yang, R. Wu, P. Ren, X. Xie, and L. Zhang, “Pixel-aware stable diffusion for realistic image super-resolution and personalized stylization,” in *Proceedings of the European Conference on Computer Vision (ECCV)*, Cham: Springer, 2025, pp. 74–91.
- [16] J. Wang, S. Wu, Z. Yuan, Q. Tong, and K. Xu, “Frequency compensated diffusion model for real-scene dehazing,” *Neural Networks*, vol. 175, p. 106281, 2024.
- [17] Y. Guo, Y. Wu, and C. Wan, “A multi-scale patch approach with diffusion model for image dehazing,” in *Proceedings of the International Conference on Intelligent Computing*, Singapore: Springer Nature Singapore, 2024, pp. 392–402.
- [18] J. Wang, Z. Yue, S. Zhou, K. C. Chan, and C. C. Loy, “Exploiting diffusion prior for real-world image super-resolution,” *International Journal of Computer Vision*, pp. 1–21, 2024.
- [19] X. Lin, J. He, Z. Chen, Z. Lyu, B. Fei, B. Dai, W. Ouyang, Y. Qiao, and C. Dong, “Diffbir: Towards blind image restoration with generative diffusion prior,” *arXiv preprint arXiv:2308.15070*, 2023.
- [20] S. Min, K. Krishna, X. Lyu, M. Lewis, W. tau Yih, P. W. Koh, M. Iyyer, L. Zettlemoyer, and H. Hajishirzi, “Factscore: Fine-grained atomic evaluation of factual precision in long-form text generation,” *arXiv preprint arXiv:2305.14251*, 2023.
- [21] J. Wang, K. C. Chan, and C. C. Loy, “Exploring clip for assessing the look and feel of images,” in *Proceedings of the AAAI Conference on Artificial Intelligence*, 2023.
- [22] M. Wang, L. Liao, D. Huang, Z. Fan, J. Zhuang, and W. Zhang, “Frequency and content dual stream network for image dehazing,” *Image and Vision Computing*, vol. 139, p. 104820, 2023. [Online]. Available: <https://www.sciencedirect.com/science/article/pii/S0262885623001944>
- [23] K. He, J. Sun, and X. Tang, “Single image haze removal using dark channel prior,” in *Proceedings of the IEEE/CVF Conference on Computer Vision and Pattern Recognition (CVPR)*, 2009, pp. 1956–1963.
- [24] H. Zhang and V. M. Patel, “Densely connected pyramid dehazing network,” in *Proceedings of the IEEE Conference on Computer Vision and Pattern Recognition (CVPR)*, June 2018.
- [25] W. Ren, S. Liu, H. Zhang, J. Pan, X. Cao, and M.-H. Yang, “Single image dehazing via multi-scale convolutional neural networks,” in *Computer Vision – ECCV 2016*, B. Leibe, J. Matas, N. Sebe, and M. Welling, Eds. Cham: Springer International Publishing, 2016, pp. 154–169.
- [26] W. Liu, X. Hou, J. Duan, and G. Qiu, “End-to-end single image fog removal using enhanced cycle consistent adversarial networks,” *IEEE Transactions on Image Processing*, vol. 29, pp. 7819–7833, 2020.
- [27] R. Wu, Z. Duan, C. Guo, Z. Chai, and C. Li, “Ridcp: Revitalizing real image dehazing via high-quality codebook priors,” in *Proceedings of the IEEE/CVF Conference on Computer Vision and Pattern Recognition (CVPR)*, 2023.
- [28] D. Zheng, X.-M. Wu, S. Yang, J. Zhang, J.-F. Hu, and W.-s. Zheng, “Selective hourglass mapping for universal image restoration based on diffusion model,” in *Proceedings of the IEEE/CVF Conference on Computer Vision and Pattern Recognition*, 2024.
- [29] Z. Yang, H. Yu, B. Li, J. Zhang, J. Huang, and F. Zhao, “Unleashing the potential of the semantic latent space in diffusion models for image dehazing,” in *Computer Vision – ECCV 2024*, A. Leonardis, E. Ricci, S. Roth, O. Russakovsky, T. Sattler, and G. Varol, Eds. Cham: Springer Nature Switzerland, 2025, pp. 371–389.
- [30] T. Schick and H. Schütze, “Exploiting cloze questions for few shot text classification and natural language inference,” *arXiv preprint arXiv:2001.07676*, 2020.
- [31] V. P. et.al, “Promptir: Prompting for all-in-one image restoration,” *Advances in Neural Information Processing Systems*, vol. 36, 2024.
- [32] S. Zhou, J. Pan, J. Shi, D. Chen, L. Qu, and J. Yang, “Seeing the unseen: A frequency prompt guided transformer for image restoration,” in *European Conference on Computer Vision (ECCV)*, 2024.
- [33] Y. Gan, Y. Bai, Y. Lou, X. Ma, R. Zhang, N. Shi, and L. Luo, “Decorate the newcomers: Visual domain prompt for continual test time adaptation,” in *Proceedings of the AAAI Conference on Artificial Intelligence*, vol. 37, no. 6, 2023, pp. 7595–7603.
- [34] M. U. Khattak, H. Rasheed, M. Maaz, S. Khan, and F. S. Khan, “Maple: Multi-modal prompt learning,” in *Proceedings of the IEEE/CVF Conference on Computer Vision and Pattern Recognition*, 2023, pp. 19 113–19 122.
- [35] C. Wang, J. Pan, W. Lin, J. Dong, W. Wang, and X.-M. Wu, “Self-promoter: Self-prompt dehazing transformers with depth-consistency,” in *Proceedings of the AAAI Conference on Artificial Intelligence*, vol. 38, no. 6, 2024, pp. 5327–5335.
- [36] C. Wang, J. Pan, W. Wang, J. Dong, M. Wang, Y. Ju, and J. Chen, “Promptrestorer: A prompting image restoration method with degradation perception,” in *Advances in Neural Information Processing Systems*, A. Oh, T. Naumann, A. Globerson, K. Saenko, M. Hardt, and S. Levine, Eds., vol. 36. Curran Associates, Inc., 2023, pp. 8898–8912.
- [37] S. Mallat, “A theory for multiresolution signal decomposition: the wavelet representation,” *IEEE Transactions on Pattern Analysis and Machine Intelligence*, vol. 11, no. 7, pp. 674–693, 1989.
- [38] L. Zhang, A. Rao, and M. Agrawala, “Adding conditional control to text-to-image diffusion models,” in *Proceedings of the IEEE/CVF International Conference on Computer Vision (ICCV)*, 2023, pp. 3836–3847.
- [39] S. Zhou, K. C. Chan, C. Li, and C. C. Loy, “Towards robust blind face restoration with codebook lookup transformer,” in *Proceedings of the 36th Conference on Neural Information Processing Systems (NeurIPS)*, 2022.
- [40] X. Chen, H. Li, M. Li, and J. Pan, “Learning a sparse transformer network for effective image deraining,” in *Proceedings of the IEEE/CVF Conference on Computer Vision and Pattern Recognition*, June 2023, pp. 5896–5905.
- [41] Z. Liu, Y. Lin, Y. Cao, H. Hu, Y. Wei, Z. Zhang, S. Lin, and B. Guo, “Swin transformer: Hierarchical vision transformer using shifted windows,” in *Proceedings of the IEEE/CVF International Conference on Computer Vision (ICCV)*, 2021, pp. 10 012–10 022.
- [42] K. Simonyan and A. Zisserman, “Very deep convolutional networks for large-scale image recognition,” *arXiv preprint arXiv:1409.1556*, 2014.
- [43] P. Esser, R. Rombach, and B. Ommer, “Taming transformers for high-resolution image synthesis,” *CoRR*, vol. abs/2012.09841, 2020. [Online]. Available: <https://arxiv.org/abs/2012.09841>
- [44] B. Li, W. Ren, D. Fu, D. Tao, D. Feng, W. Zeng, and Z. Wang, “Benchmarking single-image dehazing beyond,” *IEEE Transactions on Image Processing*, vol. 28, no. 1, pp. 492–505, 2018.
- [45] C. Ancuti, C. O. Ancuti, R. Timofte, and C. D. Vleeschouwer, “I-haze: A dehazing benchmark with real hazy and haze-free indoor images,” in *International Conference on Advanced Concepts for Intelligent Vision Systems (ACIVS)*. Springer, 2018, pp. 620–631.
- [46] C. O. Ancuti, C. Ancuti, R. Timofte, and C. D. Vleeschouwer, “O-haze: A dehazing benchmark with real hazy and haze-free outdoor images,” in *Proceedings of the IEEE Conference on Computer Vision and Pattern Recognition Workshops (CVPRW)*, 2018, pp. 754–762.
- [47] C. O. Ancuti, C. Ancuti, M. Sbert, and R. Timofte, “Dense-haze: A dehazing benchmark for image dehazing with dense-haze and haze-free images,” in *Proceedings of the IEEE International Conference on Image Processing (ICIP)*, 2019, pp. 1014–1018.
- [48] C. O. Ancuti, C. Ancuti, and R. Timofte, “Nh-haze: An image dehazing benchmark with nonhomogeneous hazy and haze-free images,” in *Proceedings of the IEEE/CVF Conference on Computer Vision and Pattern Recognition Workshops (CVPRW)*, 2020, pp. 444–445.
- [49] G. Sharma, W. Wu, and E. N. Dalal, “The ciede2000 color-difference formula: Implementation notes, supplementary test data, and mathematical observations,” *Color Research & Application*, vol. 30, no. 1, pp. 21–30, 2005.
- [50] H. Talebi and P. Milanfar, “Nima: Neural image assessment,” *IEEE Transactions on Image Processing*, vol. 27, no. 8, pp. 3998–4011, 2018.
- [51] X. Cong, J. Gui, J. Zhang, J. Hou, and H. Shen, “A semi-supervised nighttime dehazing baseline with spatial-frequency aware and realistic brightness constraint,” in *Proceedings of the IEEE/CVF Conference on Computer Vision and Pattern Recognition (CVPR)*, 2024, pp. 2631–2640.
- [52] Y. Zheng, J. Zhan, S. He, J. Dong, and Y. Du, “Curricular contrastive regularization for physics-aware single image dehazing,” in *IEEE/CVF Conference on Computer Vision and Pattern Recognition*, 2023.
- [53] Z. Chen, Z. He, and Z.-M. Lu, “Dea-net: Single image dehazing based on detail-enhanced convolution and content-guided attention,” *IEEE Transactions on Image Processing*, vol. 33, pp. 1002–1015, 2024.
- [54] Y. Cui, W. Ren, X. Cao, and A. Knoll, “Image restoration via frequency selection,” *IEEE Transactions on Pattern Analysis and Machine Intelligence*, vol. 46, no. 2, pp. 1093–1108, 2024.